One-dimensional optical thermal ratchets

2005 J. Phys.: Condens. Matter 17 S3685

(http://iopscience.iop.org/0953-8984/17/47/003)

INSTITUTE OF PHYSICS PUBLISHING JOURNAL OF PHYSICS: CONDENSED MATTER

J. Phys.: Condens. Matter **17** (2005) S3685–S3695 doi:10.1088/0953-8984/17/47/003

One-dimensional optical thermal ratchets

Sang-Hyuk Lee and David G Grier

Department of Physics and Center for Soft Matter Research, New York University, New York, NY 10003, USA

Received 6 June 2005, in final form 17 August 2005
Published 4 November 2005
Online at stacks.iop.org/JPhysCM/17/S3685

Abstract

The ability to rectify Brownian forces with spatially extended time-varying light fields creates new opportunities for studying the statistical properties of thermal ratchet models and to exploit these models' interesting and useful properties for practical applications. This paper describes experimental studies of one-dimensional thermal ratchets implemented with the holographic optical trapping technique applied to fluid-borne colloidal spheres. These studies demonstrate the complementary roles of global spatiotemporal symmetry and local dynamics in establishing the direction of ratchet-induced motion and also highlight avenues for future advances in higher-dimensional systems.

(Some figures in this article are in colour only in the electronic version)

Thermal ratchets employ time-varying potential energy landscapes to break the spatiotemporal symmetry of thermally equilibrated systems [1]. The resulting departure from equilibrium takes the form of a directed flux of energy or materials, which can be harnessed for natural processes and practical applications. Unlike conventional macroscopic machines whose efficiency is reduced by random fluctuations, thermal ratchets actually *require* noise to operate. They achieve their peak efficiency when their spatial and temporal evolution is appropriately matched to the scale of fluctuations in the heat bath.

Most thermal ratchet models involve locally asymmetric space-filling potential energy landscapes, and almost all are designed to operate in one dimension. Most practical implementations have exploited microfabricated structures such as interdigitated electrode arrays [2, 3], quantum dot arrays [4], periodic surface textures [5, 6], or microfabricated pores for hydrodynamic drift ratchets [7, 8]. Previous optical implementations have used rapidly scanned optical tweezers to create an asymmetric one-dimensional potential energy landscape in a time-averaged sense [9, 10], or a time-varying dual-well potential with two conventional optical traps [11–13].

This paper describe a broad class of optical thermal ratchets that exploit the holographic optical tweezer technique [14–20] to create large-scale dynamic potential energy landscapes. This approach permits detailed studies of the interplay of global spatiotemporal symmetry and local dynamics in establishing both the magnitude and direction of ratchet-induced fluxes. It also provides a basis for possible practical applications.

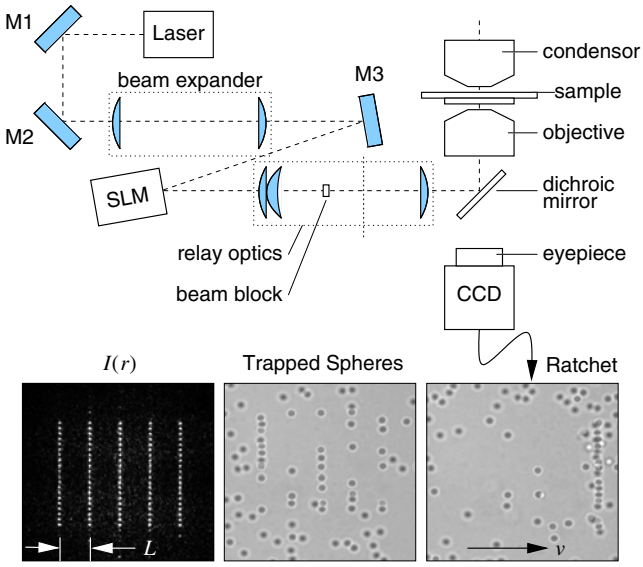

Figure 1. Schematic representation of the holographic thermal ratchet implementation.

Holographic optical tweezers use computer-generated holograms to project large arrays of single-beam optical traps. Our implementation [15], shown schematically in figure 1, uses a liquid crystal spatial light modulator (SLM) (Hamamatsu X7550 PAL-SLM) to imprint phase-only holograms on the wavefronts of a laser beam from a frequency-doubled diode-pumped solid state laser operating at 532 nm (Coherent Verdi). This SLM can vary the local phase, $\varphi(\boldsymbol{r})$, between 0 and 2π radians at each position $\boldsymbol{r}$ in a 480×480 grid spanning the beam's wavefront. The modulated beam is relayed to the input pupil of a $100\times$ NA 1.4 SPlan Apo oil immersion objective lens mounted in an inverted optical microscope (Zeiss S-100TV). The objective focuses the light into a pattern of optical traps that can be updated in real time by transmitting a new phase pattern to the SLM.

The left-most photograph in figure 1 shows the focused light, $I(\boldsymbol{r})$, from a typical pattern of holographic optical traps, which is imaged by placing a front-surface mirror on the sample stage and collecting the reflected light with the objective lens. Each focused spot of light in this 20×5 array constitutes a discrete optical tweezer [21], which acts as a spatially symmetric three-dimensional potential energy well for a micrometre-scale object. The central image in figure 1 shows an aqueous dispersion of 1.53 μm diameter colloidal silica spheres (Bangs Laboratories, lot number 5328) interacting with this pattern of traps at a projected laser power of 2.5 mW/trap.

Each potential well may be described as a rotationally symmetric Gaussian potential well [22]. Arranging the traps in closely spaced manifolds separated by a distance L creates a pseudo-one-dimensional potential energy landscape, $V(x)$, which can be modelled as

$$V(x) = -V_0 \sum_{n=-N}^{N} \exp\left(-\frac{(x - nL)^2}{2\sigma^2}\right). \tag{1}$$

The well depth, V_0, approaches the thermal energy scale, β^{-1}, when each optical tweezer is powered with somewhat less than 1 mW of light. The holographically projected traps' strengths are uniform to within ten per cent [15]. Their widths, σ, are comparable to the spheres' radii [15, 22]. With the traps powered by 3 mW, diffusing particles are rapidly

localized by the first optical tweezer they encounter, as can be seen from the centre photograph in figure 1.

The potential energy landscape created by a holographic optical tweezer array differs from most ratchet potentials in two principal respects. In the first place, the empty spaces between manifolds comprise large force-free regions. This contrasts with most models, which employ space-filling landscapes. The landscape can induce motion only if random thermal fluctuations enable particles to diffuse across force-free regions. Secondly, the landscape is spatially symmetric, both globally and locally. Breaking spatiotemporal symmetry to induce a flux rests, therefore, with the landscape's time evolution. Details of the protocol determine the nature of the induced motion.

1. Flux suppression by symmetry

The most straightforward protocols for holographic optical thermal ratchets involve cyclically translating the landscape by discrete fractions of the lattice constant L, with the nth state in each cycle having duration T_n. The motion of a Brownian particle in such a system can be described with the one-dimensional Langevin equation

$$\gamma \dot{x}(t) = -V'(x(t) - f(t)) + \xi(t), \tag{2}$$

where γ is the particle's viscous drag coefficient, the prime denotes a derivative with respect to the argument, and $\xi(t)$ is a stochastic force representing thermal noise. This white-noise forcing satisfies $\langle \xi(t) \rangle = 0$ and $\langle \xi(t)\, \xi(s) \rangle = 2(\gamma/\beta)\, \delta(t - s)$.

The potential energy landscape in our system is spatially periodic:

$$V(x + L) = V(x). \tag{3}$$

The discrete displacements in an N-state cycle, furthermore, are also described by a periodic function $f(t)$, with period $T = \sum_{n=1}^{N} T_n$. That a periodically driven, symmetric and spatially periodic potential can rectify Brownian motion to generate a directed flux might not be immediately obvious. Reimann has demonstrated [1, 23], however, that directed motion in time-evolving landscapes is all but inevitable, with flux-free operation being guaranteed only if $V(x)$ and $f(t)$ satisfy specific conditions [23] of spatiotemporal symmetry,

$$V(x) = V(-x), \qquad \text{and} \qquad \dot{f}(t) = -\dot{f}(t + T/2), \tag{4}$$

and spatiotemporal supersymmetry,

$$V(x) = -V(x + L/2), \qquad \text{and} \qquad \dot{f}(t + \Delta t) = -\dot{f}(-t), \tag{5}$$

for at least one value of Δt. The dot in equations (4) and (5) denotes a time derivative.

We will now explore two distinct classes of one-dimensional optical thermal ratchets that exploit these symmetries in different ways. The first results in directed diffusion except for a particular operating point, at which equation (4) is satisfied. The second has a point of flux-free operation even though equations (4) and (5) are always violated. In both cases, the vanishing point signals a reversal of the direction of the induced flux.

2. Two-state ratchet

The simplest optical ratchet protocol involves a two-state cycle [24],

$$f(t) = \begin{cases} 0 & 0 \leqslant (t \bmod T) < T_1 \\ \dfrac{L}{3} & T_1 \leqslant (t \bmod T) < T. \end{cases} \tag{6}$$

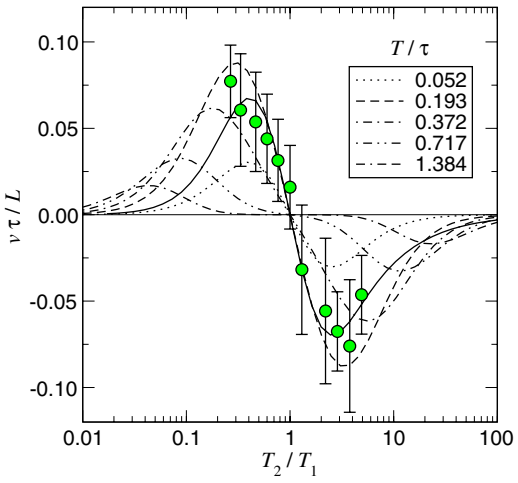

Figure 2. Flux induced by a two-state holographic optical ratchet. Discrete points show measured mean drift speed as a function of T_2 for $T_1 = 3$ s. The solid curve is a fit to the data for $\beta V_0 = 2.75$ and $\sigma = 0.65\ \mu$m. Other curves show how the induced drift depends on T/τ, with optimal flux obtained for $T/\tau = 0.193$.

In this case, $T_2 = T - T_1$. This is implemented by alternately shifting the optical trap array by one-third of a lattice constant to the right and then returning it to its initial position. Spacing the manifolds so that $L/3 \gg \sigma$ ensures that their potential wells do not overlap. Consequently, any particles localized in tweezers in one state are released into a force-free region when the landscape abruptly shifts. They subsequently diffuse freely unless they find and fall into another manifold of traps, or perhaps are recaptured when the initial state is projected again.

This protocol explicitly satisfies the symmetry condition in equation (4) when the two states are of equal duration, $T_1 = T_2 = T/2$. This particular operating point therefore should create a flux-free nonequilibrium steady-state, with particles being juggled back and forth between neighbouring manifolds of traps. Breaking spatiotemporal symmetry by setting $T_1 \neq T_2$ does not guarantee a flux, but at least creates the possibility.

The data in figure 2 demonstrate that this possibility is borne out in practice. The discrete points in figure 2 show the measured average drift velocity, v, for an ensemble of colloidal silica spheres 1.53 μm in diameter dispersed in a 40 μm thick layer of water between a coverslip and a microscope slide [24]. The spheres are roughly twice as dense as water and rapidly sediment into a free-floating layer above the coverslip [25]. The holographic optical tweezer array was projected into the layer's midplane to minimize out-of-plane fluctuations, with an estimated power of 1 mW/trap. Roughly 30 spheres were in the trapping domain at any time, so that reasonable statistics could be amassed in 10 min despite the very large fluctuations inherent in thermal ratchet operation. This number is small enough, moreover, to minimize the rate of collisions among the particles.

Given the spheres' measured diffusion coefficient of $D = 0.33\ \mu\text{m}^2\ \text{s}^{-1}$, the time required to diffuse the inter-manifold separation of $L = 5.2\ \mu$m is $\tau = L^2/(2D) = 39$ s. This establishes a natural velocity scale, L/τ, in which v is presented. These data were acquired with $T_1 = 3$ s and T_2 varying from 0.8 s to 14.7 s.

As anticipated, the ratchet-induced flux vanishes at the point of spatiotemporal symmetry, $T_2 = T_1$, and is non-zero otherwise. The vanishing point signals a reversal in the direction of the drift velocity, with particles being more likely to advance from the wells in the longer-lived state toward the nearest manifold in the shorter-lived state. This trend can be understood

as resulting from the short-duration state's biasing the diffusion of particles away from their localized distribution in the long-lived state.

To make this qualitative argument more concrete, we calculate the steady-state velocity for particles in this system by considering the evolution of the probability density $\rho(x,t)$ for finding a particle within $\mathrm{d}x$ of position x at time t. The Fokker–Planck equation associated with equation (2) is [26, 27]

$$\frac{\partial \rho(x,t)}{\partial t} = D\left[\frac{\partial^2}{\partial x^2}\rho(x,t) + \beta\,\frac{\partial}{\partial x}\left\{\rho(x,t)\,V'(x-f(t))\right\}\right]. \tag{7}$$

Equation (7) is formally solved by the master equation

$$\rho(x,t+T) = \int P(x,T|x_0,0)\,\rho(x_0,t)\,\mathrm{d}x_0 \tag{8}$$

for the evolution of the probability density, with the propagator

$$P(x,t|x_0,0) = \exp\left(\int^t L(x,t')\,\mathrm{d}t'\right)\delta(x-x_0), \tag{9}$$

describing the transfer of particles from x_0 to x under the Liouville operator

$$L(x,t) = D\left(\frac{\partial^2}{\partial x^2} + \beta\frac{\partial}{\partial x}V'(x-f(t))\right). \tag{10}$$

From equation (8), it follows that the steady-state particle distribution $\rho(x)$ is an eigenstate of the propagator,

$$\rho(x) = \int P(x,T|x_0,0)\,\rho(x_0)\,\mathrm{d}x_0, \tag{11}$$

associated with one complete cycle. The associated steady-state flux is [27]

$$v = \int \frac{x-x_0}{T}\,\rho(x_0)\,P(x,T|x_0,0)\,\mathrm{d}x\,\mathrm{d}x_0. \tag{12}$$

The solid curve in figure 2 is a fit of equation (12) to the measured particle fluxes for $\beta V_0 = 2.75$ and $\sigma = 0.65\ \mu$m. The additional curves in figure 2 show how v varies with T_1/T_2 for various values of T/τ for these control parameters. The induced flux, v, plotted in figure 3(a), falls off as $1/T$ in the limit of large T because the particles spend increasingly much of their time localized in traps. It also vanishes in the opposite limit because the diffusing particles cannot keep up with the landscape's evolution. The optimal cycle period at $T/\tau \approx 0.2$ constitutes an example of stochastic resonance [11, 12]. Although a particle's diffusivity controls the speed with which it traverses the ratchet, its direction is uniquely determined by T_2/T_1.

No flux results if the traps are too weak. Increasing the potential wells' depths increases the maximum attainable flux, but only up to a point. If the traps are too strong, particles also become localized in the short-lived state, and the ratchet approaches a deterministic flux-free limit in which particles simply hop back and forth between neighbouring manifolds. This behaviour is shown in figure 3(b).

Different objects exposed to the same time-evolving optical intensity pattern experience different values of V_0 and σ [22, 28], and also can have differing diffusive timescales, τ. Such differences establish a dispersion of mean velocities for mixtures of particles moving through the landscape that can be used to sort the particles. Despite this method's symmetry and technical simplicity, however, the two-state protocol is not the most effective platform for such practical applications. A slightly more elaborate protocol yields a thermal ratchet whose deterministic limit transports material rapidly and whose stochastic limit yields flux reversal at a point not predicted by the symmetry selection rules in equations (4) and (5).

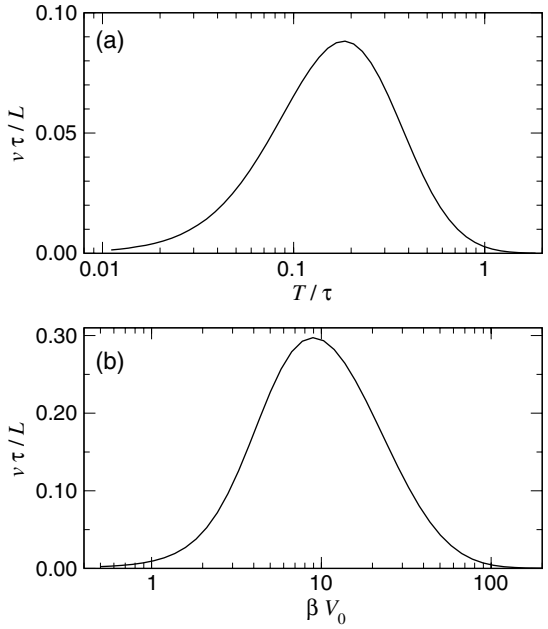

Figure 3. Stochastic resonance in the two-state optical thermal ratchet for $\sigma/L = 0.125$. (a) Dependence on cycle period T in units of the diffusive timescale τ for $\beta V_0 = 2.75$ at the optimal duty cycle $T_2/T_1 = 0.3$. (b) Dependence on well depth for the optimal cycle rate $T/\tau = 0.193$ and duty cycle.

3. Three-state ratchet

The next step up in complexity and functional richness involves the addition of a third state to the ratchet cycle:

$$f(t) = \begin{cases} 0, & 0 \leqslant (t \bmod T) < \frac{T}{3} \\ \dfrac{L}{3}, & \frac{T}{3} \leqslant (t \bmod T) < \frac{2T}{3} \\ -\dfrac{L}{3}, & \frac{2T}{3} \leqslant (t \bmod T) < T. \end{cases} \tag{13}$$

This three-state protocol [27] consists of cyclic displacements of the landscape by one-third of a lattice constant. Unlike the two-state symmetric thermal ratchet, it has a deterministic limit, an explanation of which helps to elucidate its operation in the stochastic limit.

If the width, σ, of the individual wells is comparable to the separation $L/3$ between manifolds in consecutive states, then a particle localized at the bottom of a well in one state is released near the edge of a well in the next. Provided V_0 is large enough, the particle falls to the bottom of the new well during the $T/3$ duration of the new state. This process continues through the sequence of states, and the particle is transferred deterministically forward from manifold to manifold. This deterministic process is known as optical peristalsis [29], and is useful for reorganizing fluid-borne objects over large areas with simple sequences of generic holographic trapping patterns.

Assuming the individual traps are strong enough, optical peristalsis transfers objects forward at speed $v = L/T$. If, on the other hand, $\beta V_0 \lesssim 1$, particles can be thermally

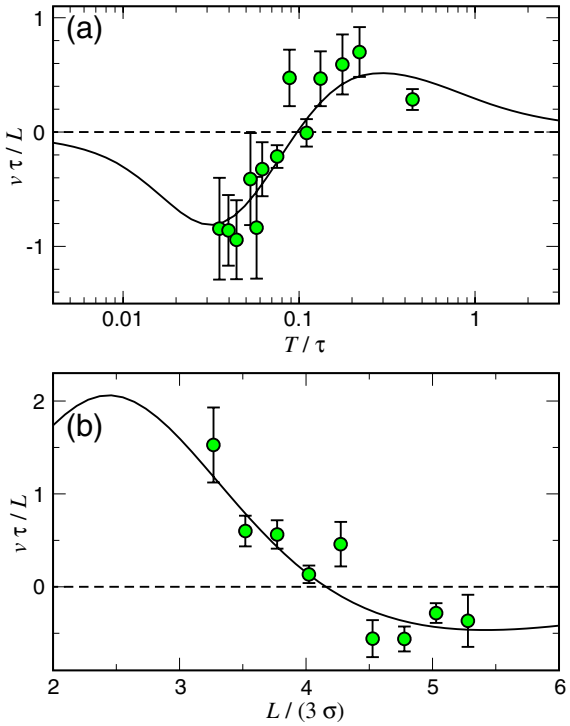

Figure 4. Flux reversal in a symmetric three-state optical thermal ratchet. (a) As a function of cycle period for fixed inter-manifold separation, L. (b) As a function of inter-manifold separation L for fixed cycle period T.

excited out of the forward-going wave of traps and so will travel forward more slowly. This is an example of a deterministic machine's efficiency being degraded by thermal fluctuations. It contrasts with the two-state thermal ratchet, which has no effect in the deterministic limit and instead relies on thermal fluctuations to induce motion.

The three-state protocol enters its stochastic regime when the inter-state displacement of manifolds, $L/3$, exceeds the individual traps' width, σ. Under these conditions, a particle that is trapped in one state is released into the force-free region between traps once the state changes. If the particle diffuses rapidly enough, it might nevertheless fall into the nearest potential well centred a distance $L/3$ away in the forward-going direction within time $T/3$. The fraction of particles achieving this will be transferred forward in each step of the cycle. This stochastic process resembles optical peristalsis, albeit with reduced efficiency. There is a substantial difference, however.

An object that does not diffuse rapidly enough to reach the nearest forward-going trap in time $T/3$ might still reach the trap centred at $-L/3$ in the third state by time $2T/3$. Such a slow-moving object would be transferred *backward* by the ratchet at velocity $v = -L/(2T)$. Unlike the two-state ratchet, whose directionality is established unambiguously by the sequence of states, the three-state ratchet's direction appears to depend also on the transported objects' mobility.

This prediction is borne out by the experimental observations [27] in figure 4. The discrete points in figure 4(a) show the measured flux of 1.53 μm diameter silica spheres as a function of the cycle period T with the inter-manifold separation fixed at $L = 6.7$ μm. Flux reversal at

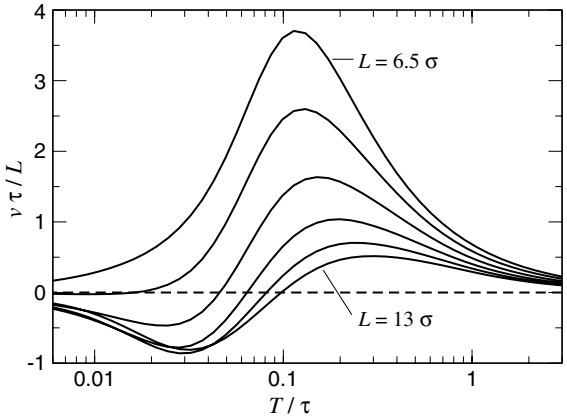

Figure 5. Calculated ratchet-induced drift velocity as a function of cycle period T for representative values of the inter-manifold separation L ranging from the deterministic limit, $L = 6.5\,\sigma$, to the stochastic limit $L = 13\,\sigma$.

$T/\tau \approx 0.1$ does not result from special symmetry considerations because the spatiotemporal evolution described by equations (1) and (13) violates the conditions in equations (4) and (5) for all values of T. Rather, this reflects a dynamical transition in which rapidly diffusing particles are driven forward while slowly diffusing particles drift backward. The origin of this transition in thermal ratchet behaviour is confirmed [1] by the observation of a comparable transition induced by varying the inter-manifold separation L for fixed cycle period $T = 6$ s, as plotted in figure 4(b) [27].

The solid curves in figure 4 are fits to equation (12) using (13) to calculate the propagator. The fit values, $\beta V_0 = 8.5 \pm 0.08$ and $\sigma = 0.53 \pm 0.01\ \mu$m, are consistent with values obtained for the two-state ratchet, given a higher laser power of 2.5 mW/trap. The crossover from deterministic optical peristalsis with uniformly forward-moving flux at small L to stochastic operation with flux reversal at larger separations is captured in the calculated drift velocities plotted in figure 5.

Whereas flux reversal in the two-state ratchet is mandated by the protocol, flux reversal in the three-state ratchet depends on properties of diffusing objects through the detailed structure of the probability distribution $\rho(x)$ under different operating conditions. The three-state optical thermal ratchet therefore provides the basis for sorting applications in which different fractions of a mixed sample are transported in opposite directions by a single time-evolving optical landscape. This builds upon previously reported ratchet-based fractionation techniques which rely on unidirectional motion [3, 30, 31].

4. Radial ratchet

The flexibility of holographic optical thermal ratchet implementations and the success of our initial studies of one-dimensional variants both invite consideration of thermal ratchet operation in higher dimensions. This is an area that has not received much attention, perhaps because of the comparative difficulty of implementing multidimensional ratchets with other techniques. As an initial step in this direction, we introduce a ratchet protocol in which manifolds of traps are organized into evenly spaced concentric rings whose radii advance through a three-state cycle analogous to that in equation (13). The probability distribution $p(\boldsymbol{r}, t)$ for a Brownian

particle to be found within d$\boldsymbol{r}$ of $\boldsymbol{r}$ at time t under external force $\boldsymbol{F}(\boldsymbol{r}, t) = -\nabla V(\boldsymbol{r}, t)$ satisfies

$$\frac{\partial p(\boldsymbol{r}, t)}{\partial t} = D\left[\nabla^2 p(\boldsymbol{r}, t) - \beta\,\nabla \cdot \{p(\boldsymbol{r}, t)\,\boldsymbol{F}(\boldsymbol{r}, t)\}\right]. \tag{14}$$

If the force depends only on the radial coordinate as $\boldsymbol{F}(\boldsymbol{r}, t) = -\partial_r V(r, t)\,\hat{\boldsymbol{r}}$, equation (14) reduces to

$$\frac{\partial p(r, t)}{\partial t} = D\left[\frac{1}{r}\frac{\partial}{\partial r}\left\{r\frac{\partial}{\partial r}p(r, t)\right\} + \frac{\beta}{r}\frac{\partial}{\partial r}\left\{r\,V'(r, t)\,p(r, t)\right\}\right]. \tag{15}$$

The probability $\rho(r, t)$ for a particle to be found between r and $r + \mathrm{d}r$ at time t is given by $\rho(r, t) = 2\pi r\,p(r, t)$. Therefore, the Fokker–Planck equation can be rewritten in terms of $\rho(r, t)$ as

$$\frac{\partial \rho(r, t)}{\partial t} = D\left[\frac{\partial^2}{\partial r^2}\rho(r, t) + \beta\frac{\partial}{\partial r}\left\{\left(V'(r, t) - \frac{1}{\beta r}\right)\rho(r, t)\right\}\right]. \tag{16}$$

This, in turn, can be reduced to the form of equation (7) by introducing the effective one-dimensional potential $V_{\mathrm{eff}}(r, t) \equiv V(r - f(t)) - \beta^{-1}\,\ln r$. The rest of the analysis follows by analogy to the linear three-state ratchet.

Like the linear variant, the three-state radial ratchet has a deterministic operating regime in which objects are clocked inward or outward depending on the sequence of states [29]. The additional geometric term in $V_{\mathrm{eff}}(r)$ and the constraint that $r > 0$ substantially affect the radial ratchet's operation in the stochastic regime by inducing a position-dependent outward drift. In particular, a particle being drawn inward by the ratchet effect must come to a rest at a radius where the ratchet-induced flux is balanced by the geometric drift. Outward-driven particles, by contrast, are excluded by the radial ratchet. Combining this effect with the three-state ratchet's natural propensity for mobility-dependent flux reversal suggests that radial ratchet protocols can be designed to sort mixtures in the field of view, expelling the unwanted fraction and concentrating the target fraction. This behaviour is successfully demonstrated in figure 6(c), in which 1 μm diameter silica spheres (Bangs Laboratories, lot number 21 024) have been collected within an outward-driving radial ratchet at $L = 4.9$ μm at $T = 4.5$ s, while larger 1.53 μm diameter silica spheres are expelled, and in figure 6(d), in which the opposite is achieved with an inward-driving ratchet at $L = 5.3$ μm and the same period, $T = 4.5$ s. A larger and more refined version might sort different fractions into concentric rings within the ratchet domain. This capability might find applications in isolating and identifying individual bacterial species within biofilms, for example.

5. Conclusions

This paper provides an overview of one-dimensional thermal ratchet models implemented with holographic optical tweezer arrays. The use of discrete optical tweezers to create extensive potential energy landscapes characterized by large numbers of locally symmetric potential energy wells provides a practical method for thermal ratchet behaviour to be induced in large numbers of diffusing objects in comparatively large volumes. The particular applications described in the preceding sections all can be reduced to one-dimensional descriptions, and are conveniently analysed with the Fokker–Planck formalism introduced in [27]. In each case, the ratchet-induced drift is marked by an operating point at which the flux reverses. In symmetric two-state travelling ratchets, flux reversal occurs at a point predicted by Reimann's symmetry selection rules [23]. The three-state variants, on the other hand, undergo flux reversal as a consequence of a competition between the landscapes' temporal evolution and the Brownian

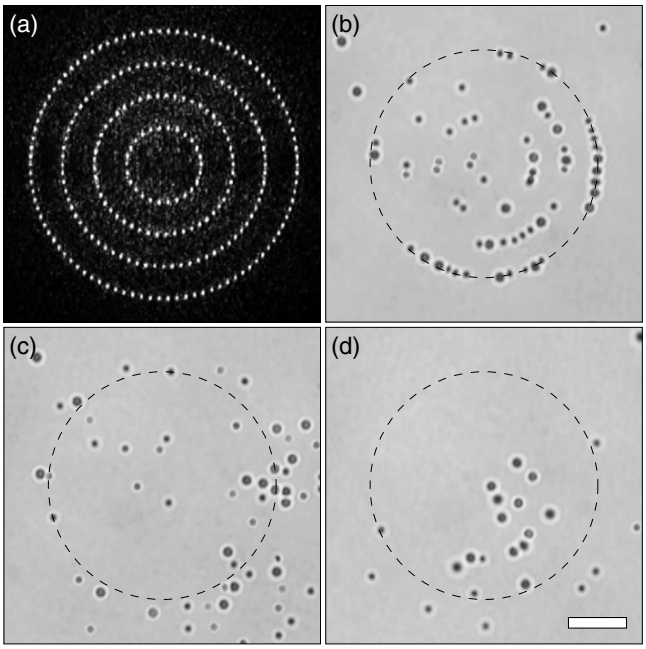

Figure 6. Fractionation in a radial optical thermal ratchet. (a) Pattern of concentric circular manifolds with $L = 4.7$ μm. (b) A mixture of large and small particles interacting with a fixed trapping pattern. (c) Small particles collected and large excluded at $L = 4.9$ μm and $T = 4.5$ s. (d) Large particles concentrated at $L = 5.3$ μm and $T = 4.5$ s. The scale bar indicates 10 μm.

particles' diffusion. The latter mechanism, in particular, suggests opportunities for practical sorting applications.

The protocols we have described can be generalized in several ways. The displacements between states, for example, could be selected to optimize transport speed or to tune the sharpness of the flux reversal transition for sorting applications. Similarly, the states in our three-state protocol need not have equal durations. They also might be tuned to optimize sorting, and perhaps to select a particular fraction from a mixture. The limiting generalization is a pseudo-continuous travelling ratchet with specified temporal evolution, $f(t)$. For simplicity, we also limited our investigation to manifolds of traps all of the same geometry and intensity. These characteristics also can be specified, with further elaborations yielding additional control over the ratchet-induced transport. It should be emphasized, however, that the conceptually and technically simple protocols described here already provide useful insights into the statistical mechanics of symmetric travelling ratchets. Despite their simplicity, moreover, they already show promise for practical applications.

Just as externally driven colloidal transport through static two-dimensional arrays of optical traps gives rise to a hierarchy of kinetically locked-in states [32–34], ratchet-induced motion through two-dimensional and three-dimensional holographic optical tweezer arrays is likely to be complex and interesting [35, 36]. Opportunities for important new insights abound because comparatively few of the proposed higher-dimensional ratchet models have been experimentally implemented. None of these, furthermore, has explored the possibilities of scaling ratchets resembling the radial ratchet introduced here but with irreducible two- or three-dimensional structure.

Acknowledgments

This work was supported by the National Science Foundation through grant number DBI-0233971. SL acknowledges support from a Kessler Family Foundation Fellowship.

References

[1] Reimann P 2002 *Phys. Rep.* **361** 57
[2] Gorre-Talini L, Spatz J P and Silberzan P 1998 *Chaos* **8** 650
[3] Bader J S, Hammond R W, Henck S A, Deem M W, McDermott G A, Bustillo J M, Simpson J W, Mulhern G T and Rothberg J M 1999 *Proc. Natl Acad. Sci.* **96** 13165
[4] Linke H, Humphrey T E, Löfgren A, Sushkov A O, Newbury R, Taylor R P and Omling P 1999 *Science* **286** 2314
[5] Carapella G, Costabile G, Martucciello N, Cirillo M, Latempa R, Polcari A and Filatrella G 2002 *Physica* C **382** 337
[6] Villegas J E, Savel'ev S, Nori F, Gonzalez E M, Anguita J V, Garcia R and Vicent J L 2003 *Science* **302** 1188
[7] Kettner C, Reimann P, Hänggi P and Müller F 2000 *Phys. Rev.* E **61** 312
[8] Matthias S and Müller F 2003 *Nature* **424** 53
[9] Faucheux L P, Stolovitzky G and Libchaber A J 1995 *Phys. Rev.* E **51** 5239
[10] Faucheux L P, Bourdieu L S, Kaplan P D and Libchaber A J 1995 *Phys. Rev. Lett.* **74** 1504
[11] McCann L I, Dykman M and Golding B 1999 *Nature* **402** 785
[12] Dykman M I, Golding B, McCann L I, Smelyanskiy V N, Luchinsky D G, Manella R and McClintock P V E 2001 *Chaos* **11** 587
[13] Dykman M I and Golding B 2000 *Stochastic Processes in Physics, Chemistry and Biology* ed J A Freund and T Pöschel (Berlin: Springer) pp 365–77
[14] Dufresne E R and Grier D G 1998 *Rev. Sci. Instrum.* **69** 1974
[15] Polin M, Ladavac K, Lee S-H, Roichman Y and Grier D G 2005 *Opt. Express* **13** 5831
[16] Grier D G 2003 *Nature* **424** 810
[17] Reicherter M, Haist T, Wagemann E U and Tiziani H J 1999 *Opt. Lett.* **24** 608
[18] Liesener J, Reicherter M, Haist T and Tiziani H J 2000 *Opt. Commun.* **185** 77
[19] Dufresne E R, Spalding G C, Dearing M T, Sheets S A and Grier D G 2001 *Rev. Sci. Instrum.* **72** 1810
[20] Curtis J E, Koss B A and Grier D G 2002 *Opt. Commun.* **207** 169
[21] Ashkin A, Dziedzic J M, Bjorkholm J E and Chu S 1986 *Opt. Lett.* **11** 288
[22] Pelton M, Ladavac K and Grier D G 2004 *Phys. Rev.* E **70** 031108
[23] Reimann P 2001 *Phys. Rev. Lett.* **86** 4992
[24] Lee S-H and Grier D G 2005 *Phys. Rev.* E **71** 060102(R)
[25] Behrens S H and Grier D G 2001 *J. Chem. Phys.* **115** 6716
[26] Risken H 1989 *The Fokker–Planck Equation* 2nd edn (Berlin: Springer)
[27] Lee S-H, Ladavac K, Polin M and Grier D G 2005 *Phys. Rev. Lett.* **94** 110601
[28] Ladavac K, Kasza K and Grier D G 2004 *Phys. Rev.* E **70** 010901(R)
[29] Koss B A and Grier D G 2003 *Appl. Phys. Lett.* **82** 3985
[30] Gorre-Talini L, Jeanjean S and Silberzan P 1997 *Phys. Rev.* E **56** 2025
[31] Bader J S, Deem M W, Hammond R W, Henck S A, Simpson J W and Rothberg J M 2002 *Appl. Phys.* A **75** 275
[32] Reichhardt C and Nori F 1999 *Phys. Rev. Lett.* **82** 414
[33] Korda P T, Taylor M B and Grier D G 2002 *Phys. Rev. Lett.* **89** 128301
[34] Gopinathan A and Grier D G 2004 *Phys. Rev. Lett.* **92** 130602
[35] Reichhardt C, Olson C J and Hastings M B 2002 *Phys. Rev. Lett.* **89** 024101
[36] Reichhardt C, Reichhardt C J O and Hastings M B 2004 *Phys. Rev.* E **69** 056115